FIBRIN AGGREGATION BEFORE SOL-GEL TRANSITION

P. WILTZIUS, G. DIETLER, W. KÄNZIG
Laboratorium für Festkörperphysik, Eidgenössische Technische Hochschule-Hönggerberg, CH-8093 Zürich, Switzerland

V. HOFMANN
Medizinische Klinik, Universitätsspital, CH-8091 Zürich, Switzerland

A. HÄBERLI AND P. W. STRAUB
Thrombose-Laboratorium, Medizinische Universitätsklinik, Inselspital, CH-3010 Bern, Switzerland

ABSTRACT Fibrinogen solutions (concentration 2 mg/ml, 0.15-M Tris-NaCl buffer, pH 7.4) were incubated at 20°C with quantities of reptilase or thrombin that were so small that the polymerization process could be followed for several hours by means of static and dynamic light scattering. The scattered intensity and its correlation function were recorded at scattering angles between 30° and 150°. The measured data were compared with model calculations based on the Flory-Stockmayer distribution, which predicts a sol-gel phase transition. This distribution is characterized by a parameter, λ, that indicates the extent of aggregation. $\lambda = 0$ corresponds to the monomeric solution, and $\lambda = 1$ indicates the sol-gel transition. Good agreement was found for monomeric units of 75-nm length aggregating (*a*) end-to-end in the early stage ($0 \leq \lambda \leq 0.3$), and (*b*) in a staggered overlap pattern for the progressing polymerization ($0.3 \leq \lambda < 1$). Before the gel point was reached, no systematic difference was observed between the data obtained after activation with thrombin, which releases both fibrinopeptides A and B from fibrinogen, and reptilase, which exclusively releases the fibrinopeptides A. This confirms that the release of the fibrinopeptides A is the essential prerequisite for the aggregation process.

INTRODUCTION

Under physiologic conditions, fibrinogen is a soluble molecule. It consists of three pairs of polypeptide chains and has a molecular weight of 330,000. The proteolytic enzyme thrombin removes two negatively charged amino-terminal peptides A (FPA) and two peptides B (FPB) per fibrinogen molecule. The kinetics of the release of the fibrinopeptides are characterized by the initial and rapid release of FPA followed, after a lag phase, by the release of FPB. From measurements of the concentration of the amino-terminal residues and light-scattering data, Blombäck and Laurent (1958) demonstrated that fibrin polymerization was correlated to the release of the fibrinopeptides. Using enzymes extracted from different snake venoms with even more specific proteolytic activity than thrombin, we found (with reptilase) that the cleavage of FPA alone was of decisive importance for the subsequent fibrin formation. The exact role of FPB has not been established yet. Herzig et al. (1970) were unable to produce fibrin strands when they used an enzyme isolated from *Agkistodron contortrix contortrix* that, at least initially, removes FPB only. In further studies, Blombäck et al. (1978) have tried to substantiate the view that FPA release was responsible for end-to-end aggregation and FPB release for side-to-side aggregation. Various degrees of staggered overlap in the oligomer strands have been proposed (Blombäck et al., 1978; Ferry et al., 1954; Bang, 1963; Kay and Cuddigan, 1967). Recently Olexa and Budzynski (1980) have reported biochemical evidence for the existence of four binding sites. In addition to the binding sites supposed to be unmasked by thrombin incubation, these authors claim to have localized attachment sites "a" and "b" already present on the parent fibrinogen molecule before enzyme activation. In their view, a and b could bind to A and B sites, respectively. Following this idea, four binding sites are already involved in the fibrinogen-fibrin aggregation process after FPA release alone. This concept is also compatible with the polymerization sets A:a and B:b as described by Blombäck et al. (1978).

The main techniques used to corroborate the polymerization models are electron microscopy (Bang, 1963; Kay and Cuddigan, 1967; Hall and Slayter, 1959), light scattering (Casassa, 1955; Müller and Burchard, 1978; Palmer and Fritz, 1979; Hantgan and Hermans, 1979), and gel permeation chromatography (Carr et al., 1977). In the first two of these methods dilute solutions of fibrinogen were commonly used, whereas the third method was used predominantly for the gel state. Palmer and Fritz (1979) analyzed a well-defined fraction of the polymer distribution with light scattering. Most of the other studies give a global characterization of the "intermediate polymers," disregarding the polymer distribution.

The fibrinogen-fibrin aggregation has been tentatively described as a bimolecular association of bifunctional units (Hantgan and Hermans, 1979; Nelb et al., 1980). The agreement of the experimental data with the predicted weight of the various polymer fractions is not satisfactory (Nelb et al., 1980). Moreover, this aggregation model cannot explain the observed sol-gel transition. It merely leads to a distribution of linear chains.

The present work contains the results of an investigation of the polymerization process by means of light scattering. The evolution of the angular dependence of the scattered intensity and of the mean line width were measured after the addition of a small quantity of either the enzyme reptilase (which releases only FPA from fibrinogen) or the enzyme thrombin (which releases the FPA and FPB). The experimental data were analyzed using model calculations based on a previous determination of the size and shape of the fibrin monomer in solution (a rodlike molecule of 75 nm length, Serrallach et al., 1979; Wiltzius and Hofmann, 1980) and on the Flory-Stockmayer distribution. In particular, end-to-end aggregation and staggered overlap were considered. Comparison of the reptilase and thrombin data clarifies the role of the release of FPA and FPB in the aggregation process.

THEORETICAL BACKGROUND

The most widely known theoretical polymer distribution that explains a sol-gel transition at a finite time is the Flory-Stockmayer distribution (Stockmayer, 1943). It describes the aggregation of molecules of the type R-A_f where each monomeric unit has f functional sites ($f \geq 3$). It can be shown that in the limit of high f the i-mer number concentrations can be written as

$$\frac{n_i}{X} = \frac{\exp(-\lambda i) \cdot (\lambda i)^{i-1}}{i \cdot i!} \tag{1}$$

where

$$X = \sum_{i=1}^{\infty} i\, n_i \tag{2}$$

is the total number of monomers initially in solution. This limit for high f is identical to the distribution found by Flory (1941) in the case of molecules of uniform length subjected to cross-linking at random. The distribution is completely characterized by a single parameter, λ, that is actually twice the number of bonds formed per monomer (for $f \gg i$). The sol-gel transition occurs at $\lambda = 1$.

The Analysis of Light-Scattering Data

In our light-scattering experiments we measured the angular dependence of the intensity and the mean Rayleigh line width of the light scattered by the polymer distribution during the aggregation process. To become aware of the difficulties and the fallacies of the data analysis, we calculated the measurable quantities for the Flory-Stockmayer distribution. In previous experiments (Serrallach et al., 1979; Wiltzius and Hofmann, 1980), it was found that fibrinogen and monomeric fibrin are elongated molecules of ~75-nm length. Moreover, we showed that the early fibrin polymerization proceeds by end-to-end aggregation (Wiltzius, 1981; Wiltzius et al., 1981). Inasmuch as the dimensions of the oligomers have the same magnitude as the wavelength of the light, the geometric arrangement of the monomeric units in the polymers manifests itself in the particle form factor. In addition to the end-to-end pattern, we take into consideration the overlap pattern proposed by Ferry et al. (1954).

There is an obvious contradiction between the Flory-Stockmayer distribution and the proposed linear aggregation models. The existence of a sol-gel transition at a finite time according to the Flory-Stockmayer distribution model is due to branching that leads to three-dimensional trees, which cannot be described by linear polymer models (end-to-end or staggered overlap). Electron micrographs of polymerized fibrin, however, clearly exhibit linear chains with little branching (Hall and Slayter, 1959; Weisel et al., 1981). Hence we will treat the light-scattering and the hydrodynamic behavior data as if the polymers were rodlike. The rod form factor and friction coefficient were taken from the literature (Broersma, 1960; Kerker, 1969). The reasons for the choice of the Flory-Stockmayer distribution are purely practical. It is the only analytical distribution known to us that describes a sol-gel transition. Nevertheless, it should be borne in mind that this distribution might be incompatible with the electron microscope observation that there is little branching.

The calculations based on Eq. 1 have been performed in the range $0 \leq \lambda \leq 0.9$, i.e., before the gel point. It was not possible to approach the limit $\lambda = 1$ more closely because of convergence difficulties. Generally, a Zimm plot is used to analyze the angular dependence of the intensity of the scattered radiation. The inverse scattered intensity is plotted vs. the square of the length of the scattering vector $\vec{q}$ (McIntyre and Gornick, 1964). $q = 4\pi n/\ell \cdot \sin\theta/2$, where ℓ is the wavelength, n the refractive index of the solution, and θ the scattering angle. The intercept at $q = 0$ yields the weight-averaged molecular weight M_w, and the slope for $q \to 0$ the "z-average" of the radius of gyration R_G. Fig. 1 represents the Zimm plot for different values of the parameter λ in the Flory-Stockmayer distribution. The data are shown for end-to-end aggregation (Fig. 1 *a*) as well as for staggered overlap (Fig. 1 *b*). The intensity is normalized to unity for $\lambda = 0$ (only monomers in the solution), and the scattering angle $\theta = 0°$. The most striking feature of this plot is the strong curvature for increasing values of λ near $q = 0$. A determination of M_w and R_G from experimental data requires knowledge of the Zimm curve at low angles. As the experimental determination of the scattered intensity at low angles ($\theta < 5°$) is subject to considerable experimental error, the analysis of

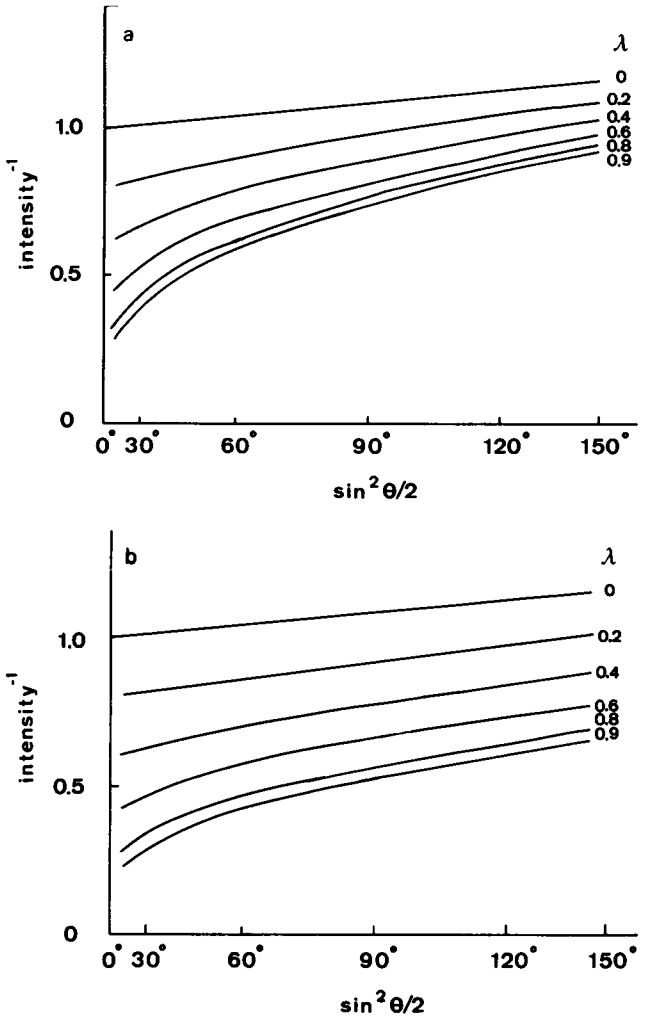

FIGURE 1 *a*, Zimm plot calculated for different values of λ in the case of end-to-end aggregation. *b*, Zimm plot calculated for different values of λ in the case of staggered overlap aggregation.

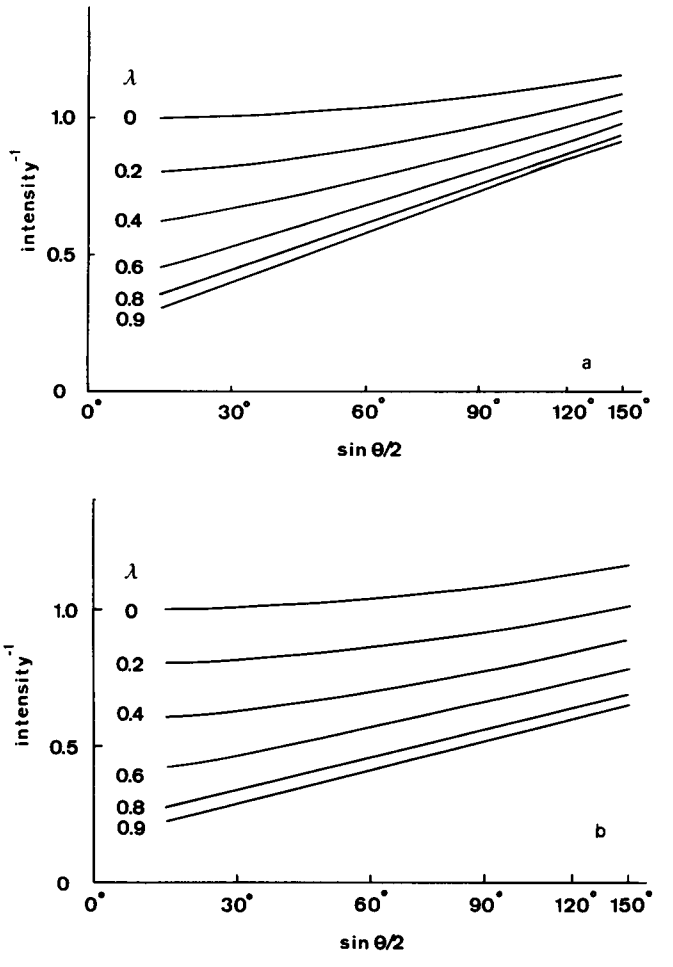

FIGURE 2 *a*, Casassa plot calculated for different values of λ in the case of end-to-end aggregation. *b*, Casassa plot calculated for different values of λ in the case of staggered overlap aggregation.

the Zimm plot becomes increasingly uncertain as the polymerization progresses.

Much more convenient for the analysis of our data is the method worked out by Casassa (1955) for polydisperse solutions of rodlike scatterers. He used an approximation formula for the particle form factor that is valid for $q \cdot L > 1.5$, where L is the length of the rod. The calculations yield a q dependence of the form

$$I^{-1}(\theta) \simeq a \cdot \left[\sum_{i=1}^{\infty} \frac{M_i w_i}{L_i^2}\right] \Big/ \left[\sum_{i=1}^{\infty} \frac{M_i w_i}{L_i}\right]^2 + b \cdot q \cdot \left[\sum_{i=1}^{\infty} \frac{M_i w_i}{L_i}\right]^{-1}. \quad (3)$$

M_i is the molecular weight of the i-mer, w_i the weight concentration, L_i the length, and a and b are constants. The calculated values of the inverse intensity are plotted vs. q in Fig. 2 for end-to-end aggregation (*a*), and for staggered overlap (*b*). For small values of λ (beginning of the aggregation process) and small scattering angles, we observe a deviation from the linear behavior predicted by Eq. 3. The agreement improves with increasing polymerization, as expected. From the slope of the curves one can deduce a weight-averaged mass per length, $\Sigma M_i w_i / L_i$. We designate the molecular weight of the monomer with M_1 and the number concentration of the i-mers with n_i to get $M_i = i \cdot M_1$ and $w_i = i \cdot n_i \cdot M_1$. For the length of the i-mer one has $L_i = i \cdot L_1$ for the end-to-end model, and $L_i = (i + 1)/2 \cdot L_1$ for the staggered overlap model where L_1 is the length of the monomer. Then

$$\sum_{i=1}^{\infty} \frac{M_i w_i}{L_i} \simeq \frac{M_1}{L_1} \sum_{i=1}^{\infty} w_i = \text{constant}. \quad (4)$$

The equality is exact for the end-to-end model. It can be seen from Fig. 2 *a* and *b* that the slope is approximately constant for values of $\lambda \lesssim 0.5$ and angles $\theta \lesssim 75°$.

For the same models we have calculated the angular dependence of the line width using the following expression

(see e.g., Berne and Pecora, 1976):

$$\bar{\Gamma} = \left[\sum_{i=1}^{\infty} M_i w_i P_i(\theta)\Gamma_i\right] \Big/ \left[\sum_{i=1}^{\infty} M_i w_i P_i(\theta)\right], \qquad (5)$$

where Γ_i is the line width attributable to the translational diffusion of the i-mers. The results are plotted in Fig. 3 as a function of the parameter λ. The differences between the two models are <3%. The line width, $\bar{\Gamma}$, drops to about half of its initial value when the gel point, $\lambda = 1$, is reached. An evaluation of the experimental results on the basis of these calculations is not feasible because the mathematics of molecular characteristics are extremely complicated. Therefore, we developed a transparent expression for the mean line width using the approximation for the particle form factor given by Casassa:

$$P_i(\theta) = \frac{\pi}{qL_i} - \frac{2}{(qL_i)^2} + \ldots . \qquad (6)$$

Using $\Gamma_i = D_i \cdot q^2$ (Berne and Pecora, 1976) and inserting Eq. 6 into Eq. 5 one obtains

$$\bar{\Gamma}(q) \simeq \left[\sum_{i=1}^{\infty} \frac{M_i w_i D_i}{L_i}\right] \Big/ \left[\sum_{i=1}^{\infty} \frac{M_i w_i}{L_i}\right] \cdot q^2 + \ldots \qquad (7)$$

where D_i is the effective translational diffusion coefficient of the i-mer. Polydisperse systems of large scatterers normally show a deviation from the linear q^2 dependence expected for monodisperse systems. Eq. 7 indicates, however, that polydisperse systems of long rodlike scatterers can show a mean line width approximately proportional to q^2. The $\bar{\Gamma}$ values calculated using the form factor and friction coefficient taken from the literature are plotted vs. q^2 in Fig. 4 for different values of λ, and show indeed the linearity expected on the basis of Eq. 7. Thus, an interpretation of the slope in terms of the simple Eq. 7 is meaningful.

The calculations of the line width (Figs. 3 and 4) only take into account the contribution due to the translational diffusion. However, one may argue that because the scatterers in a fibrinogen-fibrin solution are elongated, the contribution of the rotational diffusion to the line width has to be taken into consideration (Berne and Pecora, 1976). We have performed the same calculations as for Figs. 3 and 4 with the first-order correction term given by Pecora (1968). For the fibrinogen monomer we assumed a translational diffusion coefficient $D_T = 2 \cdot 10^{-7}$ cm^2/s and a rotational diffusion coefficient $D_R = 40{,}000\ s^{-1}$ (Serrallach et al., 1979). The contribution of the rotational diffusion to the line width is <5%. The linearity of $\bar{\Gamma}$ vs. q^2 is practically unaltered. This is because the correction term that is proportional to $(6\ D_{R_i})/(D_{T_i}q^2)$ becomes very small as i increases.

By inserting the quantities M_i, w_i, and L_i, defined earlier, into Eq. 7 and approximating the effective diffusion coefficient D_i of the i-mer by D_1/i, one obtains

$$\bar{\Gamma}(q) \simeq D_1 \cdot \sum_{i=1}^{\infty} n_i \cdot q^2 + \ldots . \qquad (8)$$

$\Sigma\, n_i$ is the total number of polymers in the solution that is the zeroth moment of the distribution. The analysis of the Flory-Stockmayer distribution shows that the total number of polymers at the gel point is equal to half the number of monomers initially present in the solution. Thus Eq. 8

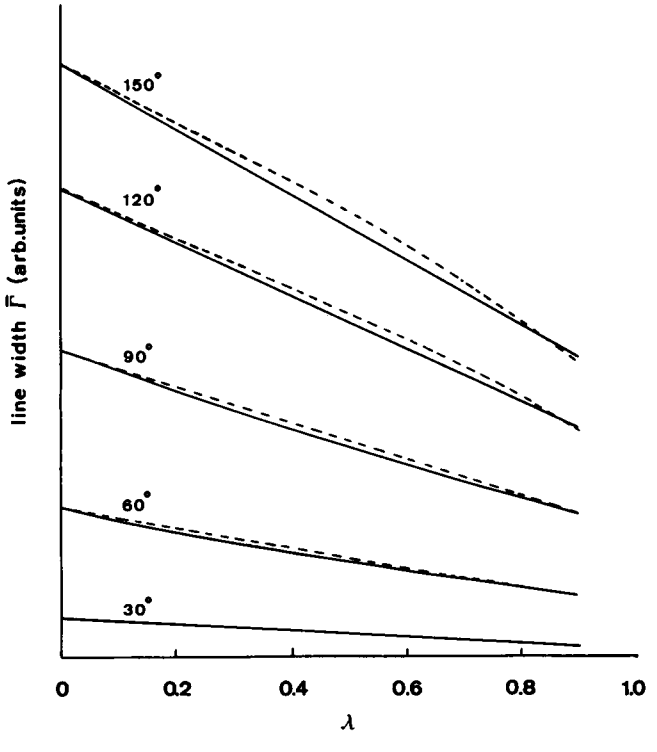

FIGURE 3 Dependence of the calculated mean line width $\bar{\Gamma}$ on the parameter λ. Solid line, end-to-end aggregation; broken line, staggered overlap aggregation model. Arb. units, arbitrary units.

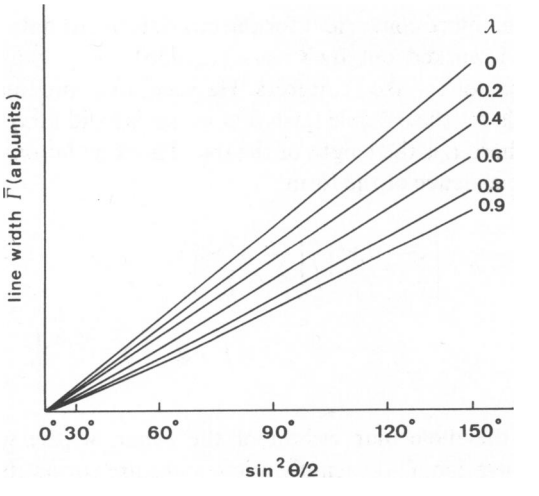

FIGURE 4 q^2 dependence of the calculated mean line width, $\bar{\Gamma}$, for different values of the parameter λ.

shows why the line width decreases to one-half of its initial value when the gel point is reached.

MATERIALS AND METHODS

Materials

Human fibrinogen (Imco, Stockholm) with clottability >95% was kept at −20°C in 1-ml portions of 2 mg/ml in a 0.05 Tris-0.1 M NaCl buffer at pH 7.4. Purified reptilase (Defibrase, batch 11-103) was obtained from Pentapharm, Basel, Switzerland. This batch has been shown to exclusively liberate FPA from fibrinogen (Blombäck et al., 1978). The reptilase was diluted 1:10 with the same buffer and stored at 4°C. Thrombin (Hoffmann-LaRoche, Basel), 100 NIH units/ml, was kept at −20°C.

Light-Scattering Apparatus and Experimental Procedure

The light-scattering apparatus has been described in detail elsewhere (Haller, 1980). The light source was an argon ion laser (Spectra-Physics, Inc., Basel) operated at $\lambda = 514.5$ nm. The digital Malvern autocorrelator (96 channels) was interfaced to a Nova 3 computer. 1 ml of the fibrinogen solution was rapidly thawed at 37°C, and 0.5 ml were transferred into a cylindrical quartz cell (8-mm i.d.). 10 μl of reptilase diluted 1:60 or 10 μl of thrombin (corresponding to 0.01 NIH units/ml), freshly prepared for each experiment, was added to the fibrinogen solution while the cell was gently shaken to avoid concentration gradients. Before the light-scattering experiments, large contaminant particles were sedimented by centrifugation at 10,000 *g* for 90 s. The measurements started 3 min after the addition of the enzyme. Because of the low enzyme concentrations, the polymerization process could be extended to 4–6 h. The scattering angles were varied between 30° and 150° in steps of 15°. Special care was taken in the adjustment of the cell for each scattering angle to avoid reflections from the cell walls. The intensity and autocorrelation function were measured during 30 s for each angle, and the data were stored in the computer. All the experiments were carried out at 20° ± 0.1°C.

Data Analysis

For the analysis of the measured autocorrelation function, two different computer programs were used. In the first the mean line width was obtained from an expansion of the autocorrelation function (including the base line) in moments of the distribution of the decay times. In the second program the base line calculated from the monitor channels of the correlator was subtracted from the measured autocorrelation function and a cumulants analysis was performed. For the data taken at the beginning of the aggregation process the results obtained by the two methods show no systematic deviation. With progressing polymerization, however, we observe that the values from the first analysis are systematically higher. The first method underestimates the contribution of the high polymers because of the finite number of channels. The second method does not have this defect because the slow decay times are correctly taken into account in the base line. Hence we present the data analyzed by the second method.

EXPERIMENTAL RESULTS

Reptilase

In Fig. 5 the measured intensities are plotted for scattering angles $30° \leq \theta \leq 135°$ and a time span of 6 h. The aggregation process was induced by the enzyme reptilase. The curves show the same characteristic behavior that has been observed in previous experiments (Wiltzius et al., 1981), i.e., an initial linear increase followed by a more rapid rise. Thus, the curves indicate that the polymerization starts immediately after enzyme

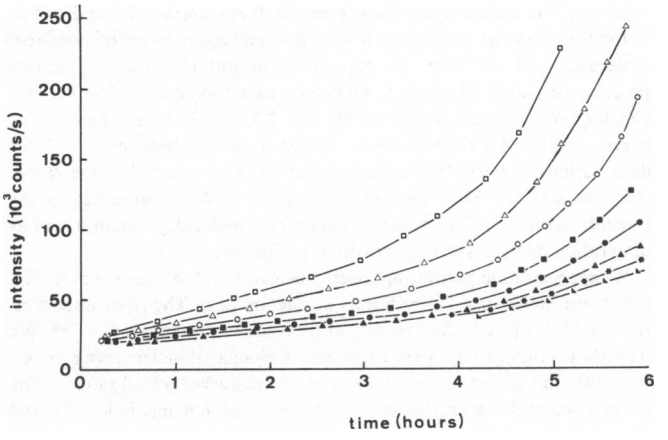

FIGURE 5 The scattered intensity, in the case of Reptilase, as a function of time for different scattering angles. □, 30°; △, 45°; ○, 60°; ■, 75°; ●, 90°; ▲, 105°; ⬟, 120°; ◣, 135°.

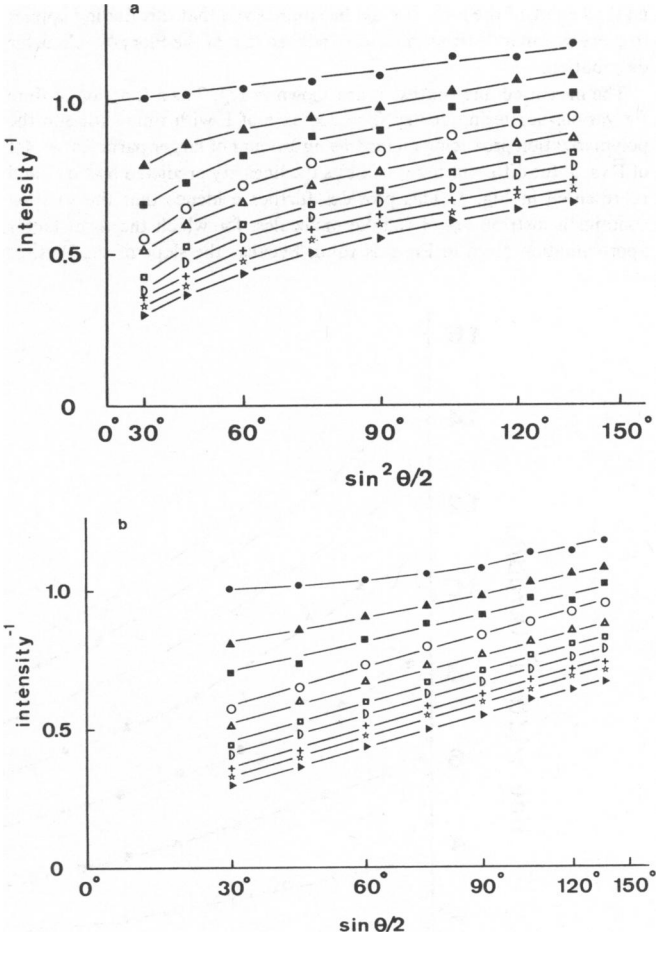

FIGURE 6 *a*, Zimm plot of the scattered intensity in the case of Reptilase for different times during the aggregation. ●, 0 s; ▲, 1,000 s; ■, 2,000 s; ○, 3,000 s; △, 4,000 s; □, 5,000 s; D, 6,000 s; +, 7,000 s; ☆, 8,000 s; ▶, 9,000 s. The intensity values at $t = 0$ have been obtained by extrapolation from Fig. 5. *b*, Casassa plot of the same intensities as in Fig. 6 *a*. The symbols indicate the following times of the aggregation process: ●, 0 s; ▲, 1,000 s; ■, 2,000 s; ○, 3,000 s; △, 4,000 s; □, 5,000 s; D, 6,000 s; +, 7,000 s; ☆, 8,000 s; ▶, 9,000 s. The intensity values at $t = 0$ have been obtained by extrapolation from Fig. 5.

addition. The initial slopes have been analyzed previously, and it was found that they can be explained by end-to-end aggregation of elongated molecules ~75 nm long. To gain more insight into the aggregation process, we plotted the inverse intensities as a function of q^2 in Fig. 6 *a* (Zimm plot). The plot represents the first 2.5 h of the measurement. The curves exhibit the characteristics expected on the basis of Fig. 1 for distributions of elongated molecules. For large q^2 values they are rather flat, but strongly bent downward for $q \to 0$. As pointed out in the theoretical section, it is unwise to determine a molecular weight or radius of gyration by means of extrapolations of this plot.

A representation permitting safer conclusions is the Casassa plot. Fig. 6 *b* shows the inverse intensities as a function of q. The most important feature of this plot is the linearity at high scattering angles $\theta > 75°$. We have shown that this has to be expected for elongated molecules aggregating either in the end-to-end mode or in the staggered overlap mode. The comparison of the intensity curves with the calculated ones in Fig. 2 *a* and *b* reveals that for $t < 2{,}000$ s (corresponding to $\lambda < 0.3$) the particles aggregate end-to-end, whereas for $t > 4{,}000$ s (corresponding to $\lambda > 0.4$) the staggered overlap mode gives better agreement. The slopes of the curves are constant for $t > 3{,}000$ s suggesting a constant mass per length according to Eq. 4. This is consistent with the staggered overlap aggregation pattern that describes a growth in the length of the aggregates with no thickening of the rods. It must be emphasized that this finding applies to every polymer distribution and is independent of the Flory-Stockmayer distribution.

The measured line widths, $\bar{\Gamma}$, are shown in Fig. 7 as a function of time for various scattering angles. The decrease of $\bar{\Gamma}$ with time is due to the polymerization producing an increasing amount of larger particles. A plot of $\bar{\Gamma}$ vs. q^2 for different times exhibits the linearity predicted by Eq. 7 and represented in Fig. 4. This provides further evidence that the solution contains a distribution of rodlike molecules, for which the form factor approximation given in Eq. 6 is valid. Because the slope of the $\bar{\Gamma}$ vs. q^2 dependence is proportional to $\Sigma\, n_i$ (Eq. 8), we can determine the time when the gel point, $\lambda = 1$, is reached. For the fibrinogen and reptilase concentrations used in the present experiments we find $t_{gel} = 2.8$ h. During this time the $\bar{\Gamma}$ values dropped to half of their initial values. A comparison of the experimental (Fig. 6 *b*) and the calculated (Fig. 2 *b*) Casassa plots indicates that the gel point deduced from the intensity measurements is $\sim t_{gel} = 10{,}000$ s or = 2.8 h. This excellent agreement of the gelation times obtained from the analyses of two independently measured quantities, line width and intensity, lends considerable support to the assumptions underlying our analysis: the Flory-Stockmayer distribution, end-to-end aggregation at the beginning of polymerization, and the staggered overlap model for the progressing polymerization.

Thrombin

The measurements with the enzyme thrombin have been performed similarly to those with reptilase. The quantity of enzyme was chosen so that the polymerization could be followed during 1 h. We preferred this time span to the 6 h chosen in the reptilase experiments because the enzymatic activity of thrombin deteriorates more rapidly. The time dependence of the measured intensities is plotted in Fig. 8. Although the aggregation proceeds faster than in the case of reptilase, the temporal evolution of the angular dependence of the scattered intensity as a function of time is very similar. The same analysis as for the reptilase experiment shows that for $t \gtrsim 10$ min the staggered overlap model of aggregation gives good agreement. The slopes of the I^{-1} vs. q curves are constant for $t \gtrsim 10$ min, suggesting a constant mass per length. Unfortunately, the aggregation proceeds too fast for an analysis of the angular dependence for times $t < 10$ min. The gelation time deduced from the Casassa plot is $t_{gel} = 30$ min.

Fig. 9 shows a plot of the line width $\bar{\Gamma}$ vs. q^2 at various stages of the aggregation process. The curves exhibit the linearity predicted by Eq. 7

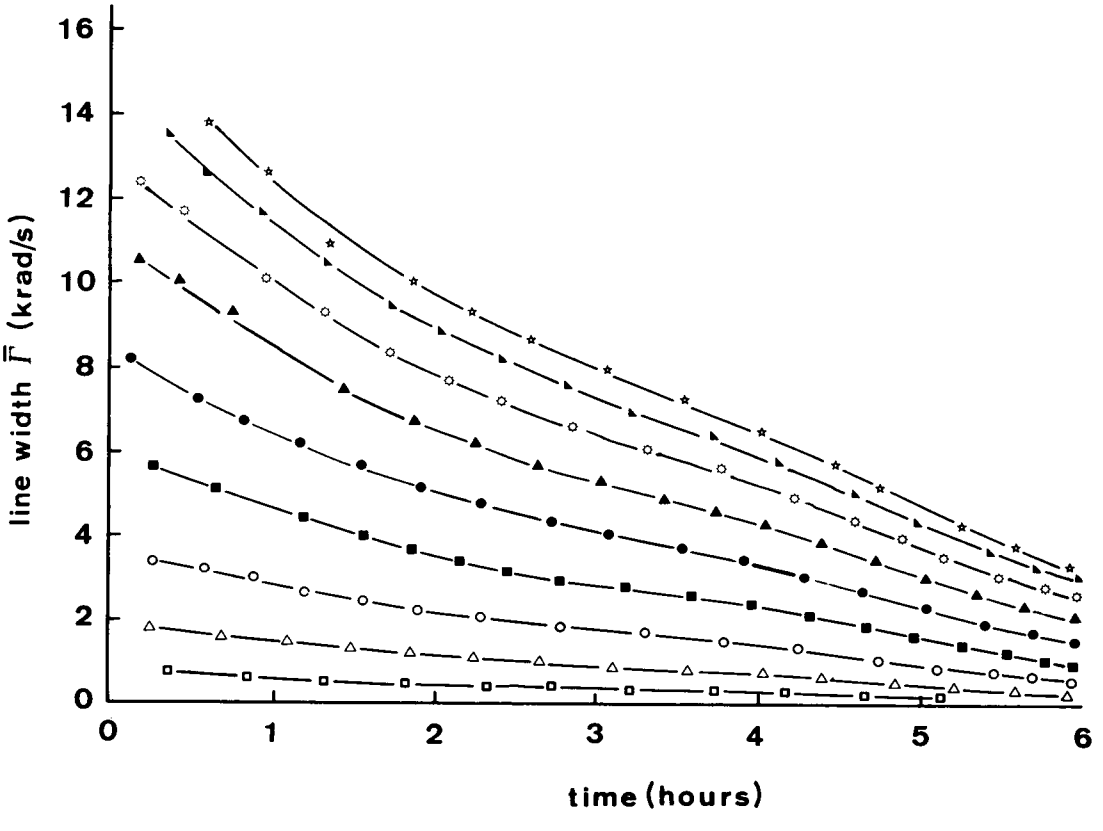

FIGURE 7 The measured line widths $\bar{\Gamma}$, in the case of Reptilase, as a function of time for different scattering angles. □, 30°; △, 45°; ○, 60°; ■, 75°; ●, 90°; ▲, 105°; ☼, 120°; ◣, 135°; ★, 150°.

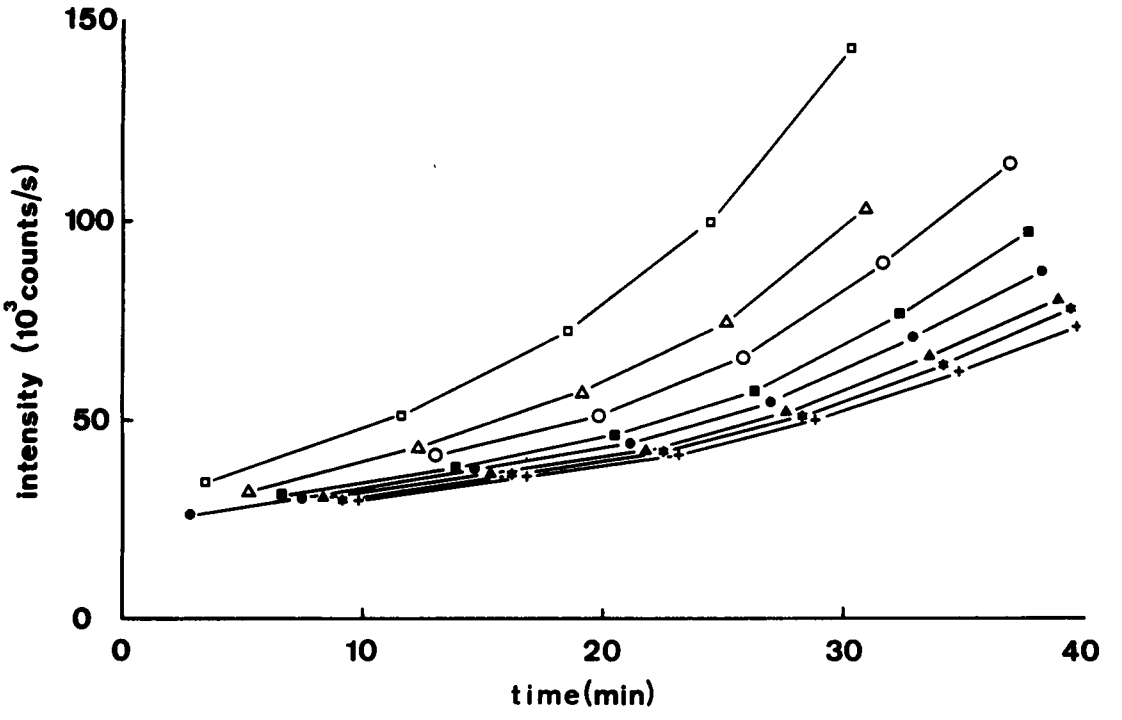

FIGURE 8 The scattered intensity, in the case of thrombin, as a function of time for different scattering angles. □, 30°; △, 45°; ○, 60°; ■, 75°; ●, 90°; ▲, 105°; ✱, 120°; +, 135°.

for a distribution of elongated particles. The gelation time obtained from this plot is t_{gel} = 30 min, which again is in agreement with t_{gel} deduced from the intensity measurements. Moreover, one can estimate a gelation time by observing the fluctuations of the forward scattered radiation on a screen. The fluctuations of the long wavelength Fourier components of the scattering density (that give rise to forward scattering) freeze in at a time close to the gelation time derived above in the data analysis.

Comparison of the Measurements Performed with Reptilase and Thrombin

The data analysis reveals a striking similarity between the aggregation induced by reptilase and by thrombin. In both cases intensity as well as line width data for $\lambda > 0.3$ are in agreement with staggered overlap, i.e., constant mass per length of the aggregates. This is surprising inasmuch as thrombin is known to split off not only FPA but also FPB from the fibrinogen molecule. The release of the latter is believed to cause lateral aggregation.

Runs with different concentrations of reptilase[1] demonstrate that by simple time-scale transformations the light-scattering data corresponding to long and short gelation times (low and high enzyme concentrations) can be compared directly for a given enzyme. The experimental data can be plotted in a way that does not depend upon the enzyme concentration. Such a plot would reveal a possible difference between the aggregation modes induced by reptilase and by thrombin.

In Fig. 10 we plot the measured $I(t)/I(0)$ vs. $\bar{\Gamma}(0)/\bar{\Gamma}(t)$ values for both enzymes for a scattering angle θ = 90°, and compare them with the calculated values for the Flory-Stockmayer distribution of polymers aggregated in an end-to-end and staggered overlap pattern. Fig. 10 reveals the same I vs. $\bar{\Gamma}$ dependence for both enzymes up to the time where $\bar{\Gamma}$ drops to about half of its initial value. For the Flory-Stockmayer distribution, and both aggregation models under consideration, this happens close to the gel point. When the aggregation proceeds beyond the gelation time, the measured intensities for thrombin exceed those for reptilase. This is consistent with the observed increasing thickness of the fibrin polymers, perhaps due to the release of the FPB. For both enzymes, the measurements of intensity and line width can be consistently explained with the following model: at the beginning the monomers aggregate end-to-end, and further polymerization can be described by a Flory-Stockmayer distribution of polymers where the monomeric units can associate in a staggered overlap arrangement. The monomeric units are 75 nm long. Side-to-side aggregation appears to occur only beyond the gelation point. An even closer agreement between the calculated and the measured data can be obtained when the calculations are performed using the following model: the dimers aggregate end-to-end, and the higher j-mers ($j \geq 3$) aggregate in a staggered overlap pattern (Fig. 10).

DISCUSSION AND CONCLUSIONS

Although a number of theoretical investigations have been performed on size distributions of aggregating polymer systems (Flory, 1941; Stockmayer, 1943; Stauffer, 1976), there is still a lack of experimental work. Recently, von Schulthess et al. (1980) reported measurements of the cluster size distributions for latex particles coated with antigen aggregating in the presence of specific antibodies. These authors found that the experimental distribution is well described by an equilibrium distribution of condensing monomers of the form A-R-B_{f-1} where each monomer has one site A and $f - 1$ B sites and bonding may take place between A and B sites. Nelb et al. (1980) compared the oligomer size distribution (obtained by gel chromatography during the fibrin aggregation) for various degrees of polymerization with the calculated distribution for bifunctional linear aggregation and found only moderate agreement. The fibrinogen to fibrin transition with subsequent

[1]Wiltzius, P. Manuscript in preparation.

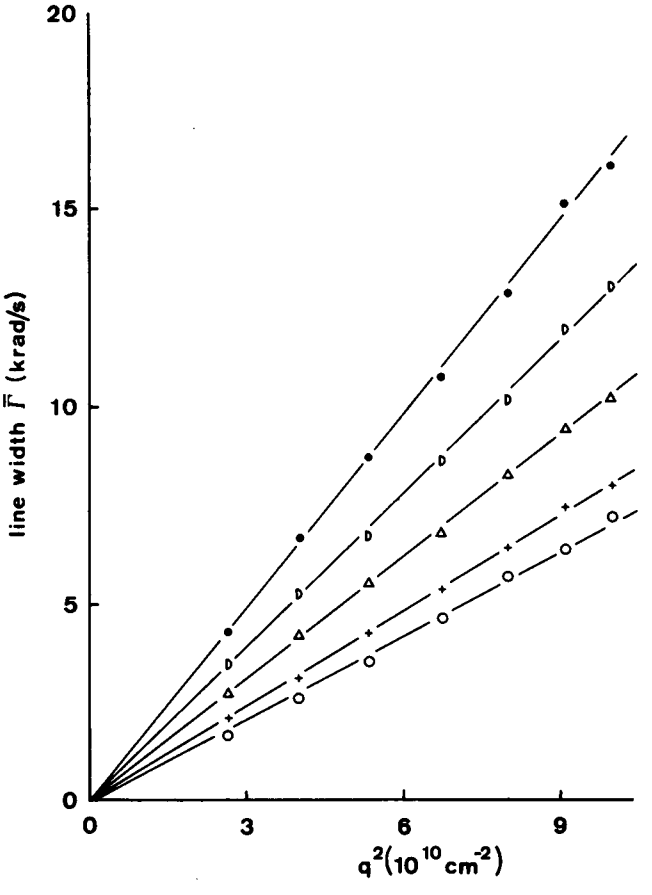

FIGURE 9 q^2 dependence of the measured mean line widths $\bar{\Gamma}$, in the case of thrombin, at different times of the aggregation process. ●, 0 min; D, 10 min; △, 20 min; +, 30 min; ○, 40 min. The line width values at $t = 0$ have been obtained by extrapolation.

aggregation is suited for experimental investigations of cluster size distributions. The aggregation in this system is governed by two principal steps. The enzymatic transformation of the soluble fibrinogen molecule to the reactive fibrin molecule through fibrinopeptide release is followed by a spontaneous polymerization. Preformed fibrin monomers devoid of the fibrinopeptides can be kept in solution at pH 4.6, but aggregate within seconds upon neutralization to form a visible clot. Because the concentrations of enzyme used in the present experiments are small, the aggregation process takes a long time. The formation of a visible clot occurs long after the completion of the measurements. Under these conditions the aggregation kinetics are mainly controlled by the enzymatic step. Therefore, the distributions can be considered to be in a quasi equilibrium during the time it takes to obtain a data point.

The fibrinogen-fibrin system exhibits a sol-gel transition at a finite time. The choice of model distributions leading to a theoretical understanding is limited by this fact. The bifunctional condensation where two reactive sites per monomer are involved in the polymerization produces linear chains only and can, therefore, be ruled out. The above mentioned A-R-B_{f-1} model yields a sol-gel transition at infinite times and thus is inadequate for the present analysis. A well-known distribution with a sol-gel point at a finite time is the Flory-Stockmayer distribution, valid for aggregating monomers of the type R-A_f, where each monomer has f functional A groups. Bonding may occur between two groups on different molecules. For the sake of simplicity we chose the high functionality limit of the Flory-Stockmayer distribution. A high functionality cannot be justified on the basis of biochemical evidence. However, calculations performed by us show that the choice of a lower functionality ($f = 4$) has only a moderate influence on the calculated intensity and line width. Moreover, we wanted to abstain from overfitting the present data; experiments designed to yield more information on this point are underway.

Considering that the release of the two FPA after the enzymatic activation with reptilase is sufficient for clot formation, and taking into account the properties of the above mentioned models, it is clear that after the release of the FPA more than two polymerization sites must be effective. Olexa and Budzynski (1980) reported evidence for two sites A and two sites a on the activated fibrin monomer, with possible interaction between A and a. A solution of activated fibrin monomers would be of the type A_2-R-a_2. Because this system is similar to the R-A_f system, one expects a gel point at a finite time.

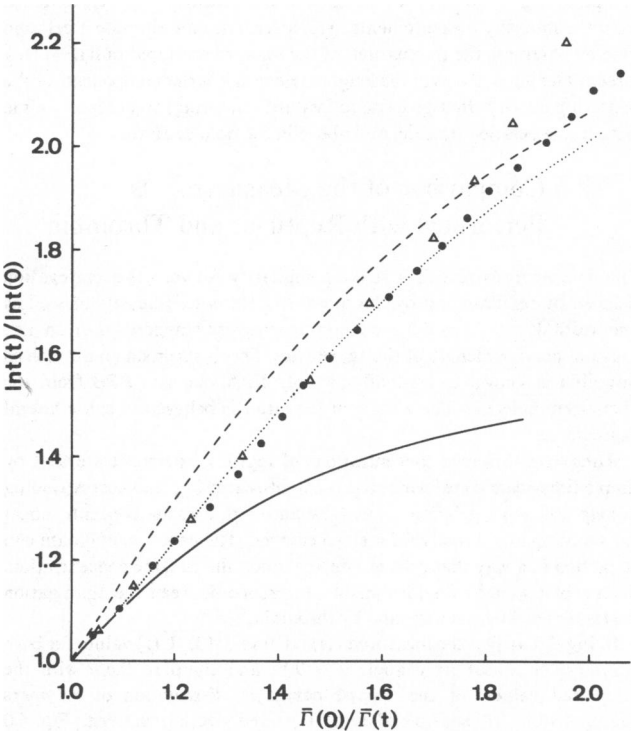

FIGURE 10 Comparison of the measured $I(t)/I(0)$ vs. $\bar{\Gamma}(0)/\bar{\Gamma}(t)$ dependence for Reptilase (●) and thrombin (△) with the calculated values for the end-to-end (solid line) and staggered overlap (broken line) aggregation models. The dotted line represents the calculated values for a Flory-Stockmayer distribution with end-to-end dimers and staggered overlapped j-mers ($j \geq 3$).

A powerful test for the applicability of a model distribution would be the measurement of the polymer size distribution. This has been performed by Nelb et al. (1980) for the first n-mers ($n < 10$). The predicted weight concentration maxima for the R-A_f distribution are 0.18 for the dimers, 0.09 for the trimers, and 0.06 for the tetramers; the initial monomer concentration is the unit. The corresponding values for the bifunctional condensation model are 0.3, 0.2, and 0.14. The comparison with the experimental results from Nelb et al. (1980), i.e., dimers 0.12, trimers 0.065, and tetramers 0.06, shows that the R-A_f distribution is in much better agreement than the bifunctional condensation model distribution. An analysis going beyond these first oligomers would require the measurement of the higher-order weight concentrations ($n < 30$) in the vicinity of the gel point to determine the critical exponents occurring in percolation and condensation theories. With the available methods (gel chromatography, Nanopar resistive pulse technique, electron microscopy) this seems to be a very difficult task.

The experimental characterization of the distributions by their moments is another test. The theoretical considerations presented in this paper show that only the zeroth moment, i.e., the number of polymers in the solution, can be determined from our experiments. Unfortunately, the data analysis designed to yield the second moment (related to the weight-averaged molecular weight, M_w, and the degree of polymerization) fails as described. We have to renounce a determination of M_w and of the radius of gyration.

Ferry et al. (1954) were the first to propose a configuration for the fibrin polymers. They suggested an end-to-end polymerization with staggered overlap, providing oligomers with a cross section twice that of fibrinogen. According to Blombäck the aggregation is correlated to the fibrinopeptide release: end-to-end after FPA release and side-by-side after FPB release (Blombäck and Laurent, 1958; Blombäck et al., 1978). Müller and Burchard (1978) concluded from static light-scattering studies that 10–12 units aggregate end-to-end before branching occurs. These authors performed their investigations with fibrinogen concentrations (0.03–0.13 mg/ml) far below the physiological concentration (2 mg/ml), so that only very fine fibrin clots were formed. Our experiments show that for values of $\lambda < 0.3$ the monomeric units aggregate in an end-to-end pattern. This is in agreement with our earlier findings (Wiltzius et al., 1981). The calculated weight-averaged molecular weight for $\lambda = 0.3$ is ~ 1.7 times the molecular weight of the fibrinogen monomer. With progressing polymerization we observe a strong deviation of the experimental intensity and line width data from the values expected for end-to-end polymerization (Casassa plots, Fig. 10). Good agreement, however, is found with the calculated values for the staggered overlap pattern for values of λ up to the gel point $\lambda = 1$.

A surprising result of the present work is that for $0 \leq \lambda < 1$ (before the gel point is reached), we find no significant differences between the data measured on fibrinogen solutions activated with reptilase or with thrombin. Hence, we can confirm that the release of FPA plays the decisive role in the gelation process. This is consistent with the finding that clots can be produced by the enzyme reptilase. In the vicinity of the gel point we begin to notice differences indicating that the thrombin induced polymers grow more thick. This is compatible with the formation of "coarse" gels with thrombin and "fine" gels with reptilase (Blombäck et al., 1978). Laurent and Blombäck (1958) carried out light-scattering experiments to compare the intermediate polymers formed after thrombin or reptilase activation. These authors evaluated their data according to Casassa (1955) and found a difference in the mass per length between thrombin formed fibrin and reptilase formed fibrin.

Although this is in disagreement with the findings of the present paper, it must be emphasized that there are crucial differences between the experiments. Laurent and Blombäck (1958) had incubation times of 18 h, providing a full conversion of fibrinogen to fibrin, whereas we analyze the earlier steps of the aggregation. In addition, the former authors carried out their experiments in 1-M urea, whereas our experiments with fibrinogen-fibrin solutions were done under physiological buffer conditions. Hence, we think that these experiments are not directly comparable to the present work.

We are presently studying the quantitative correlation between the gelation time and the amount of the released FPA. Preliminary results indicate that at the gel point a rather small amount of FPA (~35%) is split off.

The authors thank Dr. F. Leyvraz, Dr. H. R. Tschudi, Dr. N. Mazer, and Prof. Dr. G. Benedek for helpful and clarifying discussions.

This work was supported by the Swiss National Science Foundation, grant 3-938-078.

Received for publication 26 May 1981 and in revised form 20 August 1981.

REFERENCES

Bang, N. U. 1963. A molecular structural model of fibrin based on electron microscopy of fibrin polymerization. *Thromb. Diath. Haemorrh. Suppl.* 13:73–80.

Berne, B. J., and R. Pecora. 1976. Dynamic Light Scattering. John Wiley & Sons, Inc., New York.

Blombäck, B., and T. C. Laurent. 1958. N-terminal and light-scattering studies on fibrinogen and its transformation to fibrin. *Ark. Kemi.* 12:137–146.

Blombäck, B., B. Hessel, D. Hogg, and L. Therkildsen. 1978. A two-step fibrinogen-fibrin transition in blood coagulation. *Nature (Lond.).* 275:501–505.

Broersma, J. 1960. Viscous force constant for a closed cylinder. *J. Chem. Phys.* 32:1632–1635.

Carr, M. E., L. L. Shen, and J. Hermans. 1977. Mass-length ratio of fibrin fibers from gel permeation and light scattering. *Biopolymers.* 16:1–15.

Casassa, E. F. 1955. Light scattering from very long rod-like particles and an application to polymerized fibrinogen. *J. Chem. Phys.* 23:596–597.

Ferry, J. D., S. Katz, and I. Tinoco. 1954. Some aspects of the polymerization of fibrinogen. *J. Polym. Sci.* 12:509–516.

Flory, P. J. 1941. Molecular size distribution in three dimensional polymers. III. Tetrafunctional branching units. *J. Am. Chem. Soc.* 63:3096–3100.

Hall, C. E., and H. S. Slayter. 1959. The fibrinogen molecule: its size, shape, and mode of polymerization. *Biophys. Biochem. Cytol.* 5:11–15.

Haller, H. R. 1980. The application of dynamic light scattering and fluorescence depolarization to the determination of macromolecular binding characteristic. Ph.D. Thesis. Eidgenössische Technische Hochschule. Zürich, Switzerland. Thesis No. 6604.

Hantgan, R. R., and J. Hermans. 1979. Assembly of fibrin. A light scattering study. *J. Biol. Chem.* 254:11272–11281.

Herzig, R. H., O. D. Ratnoff, and J. R. Shainoff. 1970. *J. Lab. Clin. Med.* 76:451–465.

Kay, D., and J. Cuddigan. 1967. The fine structure of fibrin. *Br. J. Haematol.* 13:341–347.

Kerker, M. 1969. The Scattering of Light. Academic Press, Inc., New York.

Laurent, T. C., and B. Blombäck. 1958. On the significance of the release of two different peptides from fibrinogen during clotting. *Acta Chem. Scand.* 12:1875–1877.

McIntyre, D., and F. Gornick, editors. 1964. Light Scattering from Dilute Polymer Solutions. Gordon and Breach, Science Publishers, Inc., New York.

Müller, M., and W. Burchard. 1978. Fibrinogen-fibrin transformations characterized during the course of reaction by their intermediate structures. *Biochim. Biophys. Acta.* 537:208–225.

Nelb, G. W., G. W. Kamykowski, and J. D. Ferry. 1980. Kinetics of ligation of fibrin oligomers. *J. Biol. Chem.* 225:6398–6402.

Olexa, S. A., and A. Z. Budzynski. 1980. Evidence for four different polymerization sites involved in human fibrin formation. *Proc. Natl. Acad. Sci. U. S. A.* 77:1374–1378.

Palmer, G. R., and O. G. Fritz. 1979. Quasielastic light-scattering studies on human fibrinogen and fibrin. II. Fibrin polymerization. *Biopolymers.* 18:1659–1672.

Pecora, R. 1968. Spectral distribution of light scattered by monodisperse rigid rods. *J. Chem. Phys.* 48:4126–4128.

Serrallach, E. N., V. E. Hofmann, M. Zulauf, T. Binkert, R. Hofmann, W. Känzig, P. W. Straub, and R. Schwyzer. 1979. Fibrinogen: agreement of experimental and calculated hydrodynamic data with electron-microscopic models. *Thromb. Haemostasis.* 41:648–654.

Stauffer, D. 1976. Gelation in concentrated critically branched polymer solutions. *J. Chem. Soc. Faraday Trans. II.* 72:1354–1364.

Stockmayer, W. H. 1943. Theory of molecular size distribution and gel formation in branched-chain polymers. *J. Chem. Phys.* 11:45–55.

von Schulthess, G. K., G. B. Benedek, and R. W. DeBlois. 1980. Measurement of the cluster size distribution for high functionality antigens cross-linked by antibody. *Macromolecules.* 13:939–945.

Weisel, J. W., G. N. Phillips, and C. Cohen. 1981. A model from electron microscopy for the molecular structure of fibrinogen and fibrin. *Nature (Lond.).* 289:263–267.

Wiltzius, P., and V. Hofmann. 1980. Conformational identity of fibrinogen and fibrin monomer. *Thromb. Res.* 19:793–798.

Wiltzius, P. 1981. An investigation of the fibrinogen to fibrin transition by means of light scattering. Ph.D. Thesis. Eidgenössische Technische Hochschule. Zürich, Switzerland. Thesis No. 6764.

Wiltzius, P., V. Hofmann, P. W. Straub, and W. Känzig. 1981. The early stages of the fibrinogen-fibrin transition. *Biopolymers.* 20:2035–2049.